Enhancing the Accuracy of A-ROM Measurements for Finger Joint Angles using Image Processing and Automated Computation

Huu Hieu Quang
Department of Electrical and Mechanical Engineering, Nagoya Institute of Technology, Nagoya, Aichi 466-8555, Japan
31513006@stn.nitech.ac.jp (corresponding author)

Yoshifumi Morita
Department of Electrical and Mechanical Engineering, Nagoya Institute of Technology, Nagoya, Aichi 466-8555, Japan
morita@nitech.ac.jp

Noritaka Sato
Department of Electrical and Mechanical Engineering, Nagoya Institute of Technology, Nagoya, Aichi 466-8555, Japan
sato.noritaka@stn.nitech.ac.jp

Makoto Takekawa
Everfine LLC, Kuwana, Mie 511-0851, Japan
makoto.takekawa@gmail.com

Received: 25 February 2025 | Revised: 04 April 2025 | Accepted: 06 April 2025

 DOI: https://doi.org/10.48084/etasr.8926

ABSTRACT

In our previous research, we developed a technique for quantifying finger joint angles to assist rehabilitation therapists in assessing patients' Active Range of Motion (A-ROM). Therapists often face the challenge of accurately adjusting camera orientations (roll, yaw, pitch) to precisely capture finger joints. Our previous approach, a deep learning-based "posture determination method," required extensive training data to achieve accuracy. Moreover, accurately determining the 3D centerline of a finger proved difficult due to the limitations of the Hand Keypoint (HKP) method. Deviations in the camera pitch angle from 0° introduced distortions in the Point Cloud Data (PCD), necessitating repeated captures and thus reducing efficiency without effectively addressing the distortion. To address these limitations, we introduce several methodological advancements in this study. First, we implement a new "posture determination method" that utilizes image processing to reduce the reliance on large training datasets. Second, we enhance the accuracy of the centerline measurement by developing a calculation method that utilizes joint positions derived from image processing. Lastly, we establish a technique to correct distortions in the PCD of the centerline measurement, including adjusting the pitch angle back to 0°, thereby compensating for any data distortion. The new method was validated on five healthy participants and achieved a mean absolute error of 1.3° in the measurement of finger joint angles, which satisfies the accuracy requirement of 2°. In addition, the average measurement time was significantly reduced from 4.9 s with the previous method to 1.3 s.

Keywords-range of motion; rehabilitation; goniometer; depth camera; image processing

I. INTRODUCTION

Assessment of therapy effectiveness in rehabilitation clinics often includes measuring patients' Active Range of Motion (A-ROM) using a traditional goniometer. Authors in [1] and [2] suggested using this conventional device to directly record the A-ROM of patients' limbs. However, such devices can prolong the measurement time and potentially burden the patient. Research categorizes devices used to measure the A-ROM of finger joints into two types: contact and contactless. In clinical

settings, a goniometer ruler, which is a contact device, is commonly used. However, aligning the goniometer ruler directly with the finger joint axis can cause discomfort to patients. To minimize force application during A-ROM measurements, alternative approaches involve attaching small objects such as strain sensors, accelerometers, or markers for motion capture systems to the skin instead of using a goniometer [3-5]. Various studies have explored rehabilitation techniques aimed at restoring motor functions using different measurement methodologies [6-7]. Motion capture systems, often used for limbs, also employ markers attached to finger joints. In addition, strain sensors have been used to measure finger joint angles [8, 9], with authors in [10] and [11] reporting measurement errors of 1.63° and 3.5°, respectively. However, these methods still require skin contact and can be time consuming and cumbersome, especially when assessing multiple finger joints.

Conversely, as a contactless alternative, some researchers have developed measurement systems using an RGB-D camera, which combines an RGB camera with a depth sensor. This method is minimally invasive to the patient, but presents challenges in achieving the precision required for rehabilitation. Numerous studies have attempted to improve the effectiveness of RGB-D camera systems. For instance, authors in [12] introduced new user interface elements by employing a depth camera on a tablet to gather input information. This contactless approach addresses the issues associated with contact methods, which can increase patient discomfort during measurements. However, the Root Mean Square Error (RMSE) of the measured joint angles was 10°, which does not meet the less than 2° error requirement for hand therapy. Authors in [13] utilized an RGB camera as a contactless measurement device, but the average mean error recorded was 4.757°, failing to meet the precision standards necessary for hand therapy.

In our previous study in [14] an alternative method was suggested in which therapists measured the joint angles of a virtual 3D finger reconstructed from the Point Cloud Data (PCD) captured by an RGB-D camera. Despite this advanced approach, the maximum error reached 6.6°, which also did not meet the stringent accuracy requirements for therapeutic applications. Our previous method exhibits three significant limitations. The first is the difficulty therapists encounter when adjusting the camera's orientation (roll, yaw, and pitch) to optimally capture finger joints, as illustrated in Figure 1. To address this challenge, it is critical to verify the accuracy of the camera posture from the images captured by the device. Previously, a "posture determination method" using the Single Shot MultiBox Detector (SSD) algorithm from deep learning techniques was developed to adjust the camera's roll and yaw [15]. However, the preparation of large amounts of training data in advance is a major challenge. Second, it is essential for therapists to obtain three-dimensional data of the measurement centerline, which is defined as the central line along which the goniometer is applied to the joint under examination. Previously, a measurement centerline calculation method utilizing a Hand Keypoint (HKP) was introduced to determine the necessary joint position for centerline calculations [15]. Yet, the accuracy of joint position measurements using the HKP was insufficient. Third, therapists face difficulties in adjusting the pitch angle to 0° when aligning the camera with their fingers. Additionally, distortions occur in the PCD of the measurement centerline when the pitch angle deviates from 0°. Previously, to address the first issue, a protocol was established to request a recapture whenever the pitch angle was not at 0° [15]. Despite this measure, the frequency of recaptures was high, and the issue of data distortion remained unresolved.

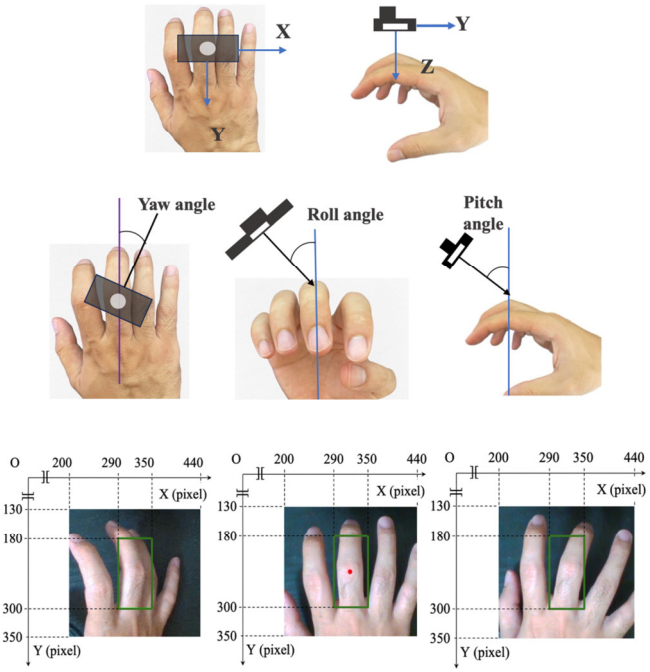

Fig. 1. Spatial arrangement between the RGB-D camera and the target joint.

In this study, we present a novel method for detecting the A-ROM of finger joints to address these issues and to validate the effectiveness of this method through experimental trials on five healthy participants. To address the first issue, we have developed a "camera posture determination method" that utilizes image processing to eliminate the necessity for extensive training data preparation. To address the second issue, we introduce a centerline measurement calculation method that utilizes joint position data obtained through image processing, thereby enhancing the accuracy of these measurements. For the third issue, we have engineered a method to correct the PCD of the measurement centerline, which includes adjustments to achieve a pitch angle of 0° and corrections for PCD distortion.

II. A-ROM CALCULATION METHOD

The methodology for calculating the A-ROM of the target joint in four fingers (excluding the thumb, which is not considered in this method) follows the framework established in our previous study, but incorporates different approaches, as depicted in the flowchart in Figure 2. Initially, the therapist captures an image of the target finger joint using an RGB-D camera, specifically the Intel RealSense camera SR300, hereafter referred to as the camera. The final step, "Calculate A-ROM," depicted in Figure 2 and employed in both our

previous and current methods, requires that the relative posture between the camera and the finger be close to 0°. This relative posture is defined by three angles: roll, pitch, and yaw, as indicated in Figure 1. A green box appears on the image display when the therapist captures the finger joint image, as shown at the bottom of Figure 1, to assist the therapist in ensuring that the roll and yaw angles are both 0°.

After the image is captured, the proposed method evaluates the roll and yaw angles. In our previous research, an SSD algorithm trained on 600 images was used to detect these angles. To address the challenge of limited training data, this study employs an Image Processing Algorithm (IPA), as described in Section II.A. If the roll and yaw angles are not nearly 0°, the image must be recaptured. A state where the roll and yaw angles are close to 0° is considered "proper." An image captured in this proper posture is then used to identify the center point, as detailed in Section II.B.

To calculate the angle of the target joint, it is essential to acquire the 3D coordinates in the PCD of the measurement centerline. The process for this conversion remains the same as described in our previous study [15]. However, distortion in the PCDs can compromise the accuracy of the A-ROM calculation, and several studies have identified distortion as a significant factor [16-20]. Achieving a pitch angle of 0° is crucial for minimizing errors during the conversion step. Previously, if the pitch angle was not close to 0°, the target joint image had to be recaptured and the procedure restarted, which was time consuming. To enhance the accuracy of the A-ROM calculation and reduce the measurement time, this study introduces a new method in Section II.C to automatically compute and convert inappropriate PCDs on the measurement line.

A. Determining The Proper Camera Posture

This subsection elaborates on the methodology employed to determine the appropriateness of the posture captured by the camera, which varies for each of the three joints: Distal Interphalangeal (DIP), Proximal Interphalangeal (PIP), and Metacarpophalangeal (MP).

In scenarios where the relative posture is considered appropriate, the camera's vertical axis is aligned parallel to the fingerbone's long axis. The process for determining proper alignment involves several steps: Initially, the therapist selects one of four finger types and one of three joint types for imaging within the green box. For example, as shown in Figure 3, the index finger was selected, with the DIP, PIP, and MP joints shown from left to right. The dimensions of the green box were set to 100 × 60 pixels, 120 × 60 pixels, and 150 × 60 pixels for the DIP, PIP, and MP joints, respectively. The image within the green box was cropped as depicted in Figure 3(a), and used to assess whether the posture was proper or improper, as detailed in Section II.B. The contour of the finger was extracted from the cropped image, as illustrated in Figure 3(b). If the absolute difference in x-coordinates between the start and end points of the vertical green line is 2 pixels or less, the posture is considered proper; otherwise, it is considered improper, as shown in Figure 3(c). The centerline is defined as the line running along the longitudinal axis of the bones forming the target joint. For the PIP and MP joints, the finger contour could not be completely captured within the boundaries of the green box. Therefore, the x-coordinates of the midpoints of line segments parallel to the x-axis were calculated. These midpoints and line segments are illustrated in Figure 3(c) as red dots and blue lines, respectively. The y-coordinates for these segments were selected randomly, with the number of segments set to 50 for the PIP joint and 25 for the MP joint. To minimize the influence of adjacent finger contours, the start and end points of each line segment were chosen from points on the contour closest to the left and right sides of the image centerline, respectively. If the range of the x-coordinates of all midpoints was within two pixels, the camera posture was considered proper.

B. Center Point Detection

The centerline of the DIP joint is derived from the previously described results. The centerlines for the PIP and MP joints are approximated from the midpoints of the line segments. The x-coordinates of the center points are determined from the centerlines indicated by the green lines in Figure 3(c). This discussion will now focus on the methodology for determining the y-coordinates of these center points.

In this study, it is postulated that the center point of each joint in the image is located at the center of visible skin folds or wrinkles. To identify these, the image undergoes a process to extract only the wrinkles, from which the y-coordinates of the center point are calculated. Wrinkle extraction is performed in two steps. First, the image colors are converted from RGB to HSV (Hue, Saturation, Value) to distinguish between similar colors, such as those of nails and skin. The image brightness is assessed using the value component of the HSV scale. If the average value (V) of all pixels in the image is greater than 230, the image is considered too bright; conversely, if the V value is less than70, the image is considered too dark. In cases where the image is too dark or too bright, the therapist is advised to recapture the image. Following this, the background is eliminated using the hue component. For instance, for the DIP joint, if the average hue value for an individual's finger skin around the target joint is represented as H, and the hue value for the n-th pixel is $H(n)$, pixels within the range of H-10 to H+20 are identified as the skin area, whereas all others are classified as background. Specifically, for the DIP joint, it is also necessary to exclude the nail region, which is done using the saturation values: the typical saturation range for skin is between 40 and 80, whereas for nails it is between 20 and 30. The average saturation value of the skin surrounding the target joint is used to differentiate and remove pixels attributed to the nail, ensuring that only the relevant finger area is analyzed. Further details on the determination of HSV values around the target joint for each person will be discussed below.

Second, a Sobel filter was applied to highlight the wrinkles on each target joint. Non-horizontal ridges, often resulting from noise or irrelevant details, were filtered out for the DIP and PIP joints, as wrinkles in these areas typically manifest as horizontal lines. Ridges exceeding seven pixels in height were excluded from the analysis. After these refinement steps, the

wrinkle points were successfully identified, as illustrated in Figure 4(b), where the red pixels denote the detected wrinkles.

Subsequently, the average y-coordinate of the wrinkle pixels located along the centerline was calculated to determine the y-coordinate of the center point of the target joint in the image. This center point is marked by a small red circle in Figure 4(c). Furthermore, a line connecting two points, positioned 30 pixels above and below the joint center point along the centerline, was designated as the measurement centerline. The PCD corresponding to the pixels along this measurement centerline is utilized in calculating the A-ROM, as detailed in the box labeled "Translate 2D to 3D with depth data" in Figure 2.

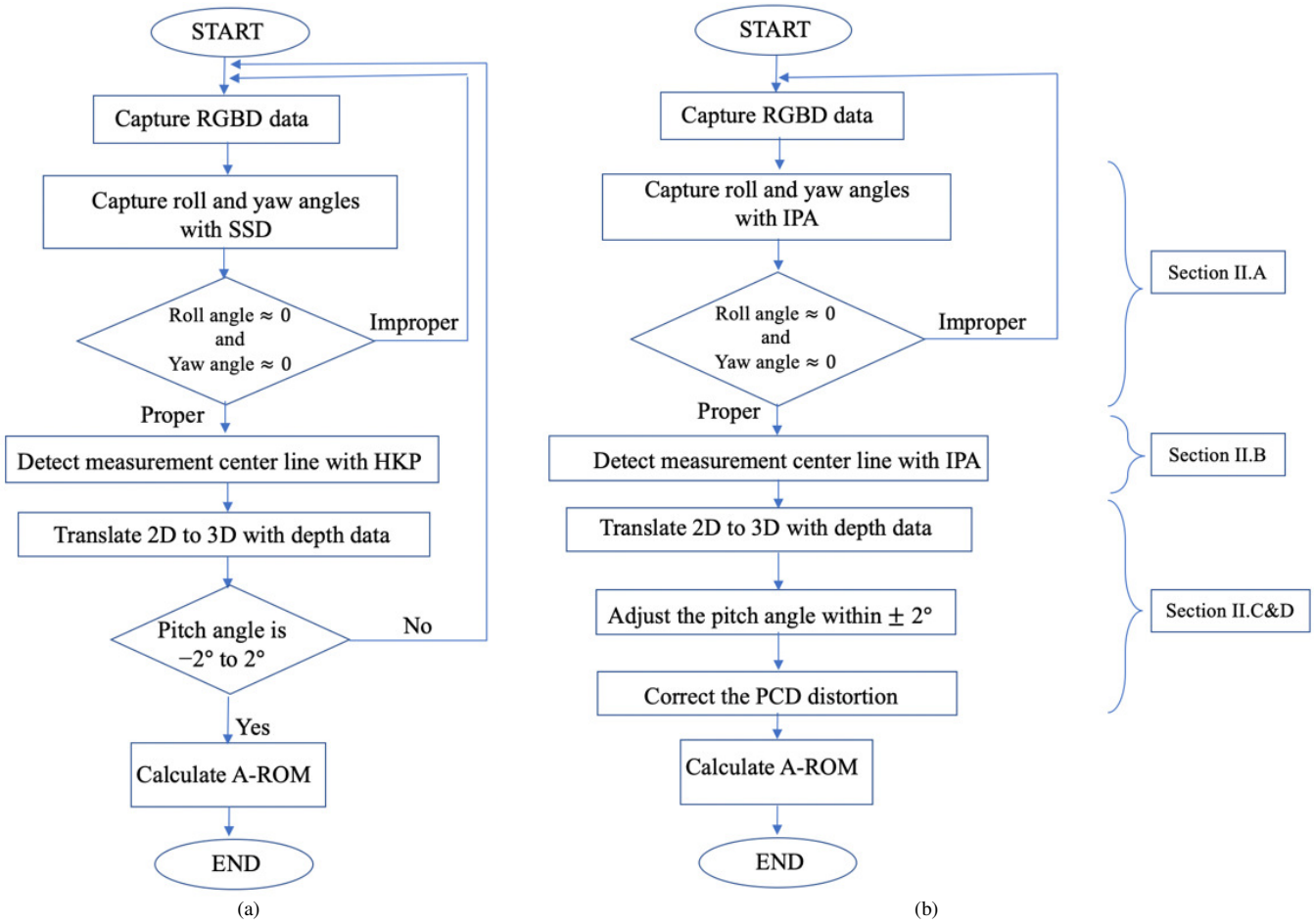

Fig. 2. Flowcharts of the A-ROM calculation procedures for the previous and proposed methods: (a) previous method, (b) proposed method.

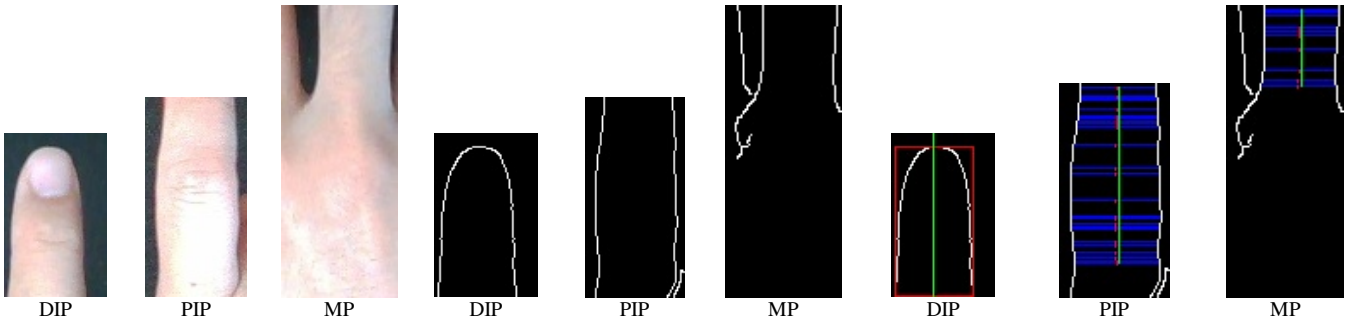

Fig. 3. Process of determining the properness of the relative camera posture and the center lines of the fingers for the DIP, PIP, and MP joints: (a) cropped original images, (b) edge detection images where the white line represents the extracted finger contour of the finger, and (c) images showing the centerlines where the red box represents the smallest possible area that covers the contour line of the finger, the blue horizontal lines are line segments, the red points are the midpoints of each line segment, and the green lines are estimated center lines of the fingers.

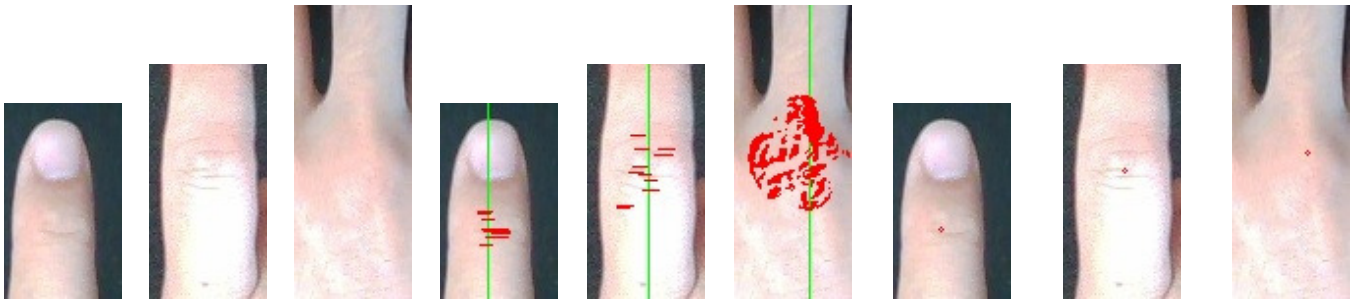

Fig. 4. Process for determining the y-coordinates of the DIP, PIP, and MP joints: (a) cropped original images, (b) ridge points and centerline, and (c) center point of joint.

As outlined in the initial step, individual HSV parameters were used to extract the skin region. Due to variations in hand color among individuals, a parameter table consisting of nine rows and four columns was created for each participant. The rows include the *H*, *S*, and *V* parameters for each of the three joints: DIP, PIP, and MP. The columns correspond to the four different finger types, ranging from the index finger to the little finger. Each cell in the table represents the average *H*, *S*, and *V* values for each joint of each finger type. The three-step process for obtaining these values is described as follows:

- First, a database was created to collect and store the names, ages, and genders of the participants. Image quality is assessed for adequate brightness using the *V* component, as previously described.
- Next, the image of the participant's hand is displayed on a Graphical User Interface (GUI), and the therapist clicks near the center of each of the 12 joints on the image to identify the fingers and joints during the examination. The coordinates of these joints are then stored in a coordinate list. For each joint, a circle with a 35-pixel radius is cropped from the image, centered at the click point, and the color within this circle is converted from RGB to HSV.
- Finally, the average *H*, *S*, and *V* values for each cropped circle are recorded in the user's database. These values are crucial for accurately extracting the skin region while taking into account individual variations in skin color.

C. Correction for PCD Distortion and Calculation Method of Joint Angle

The method for calculating the joint angle, as proposed in previous studies, utilizes the PCD from the measurement centerline. It is essential to maintain the pitch angle of the camera close to 0°. While therapists can relatively easily adjust the roll and yaw angles by viewing the RGB camera images, adjusting the pitch angle poses challenges due to limited visibility. Moreover, these adjustments are time consuming, which highlights the need to reduce measurement time as a goal for future improvements [15]. When the pitch angle deviates from 0°, not only is the PCD corrected to a 0° pitch angle, but also, if the pitch angle is not precisely 0°, the PCD distribution becomes distorted. Simply rotating the pitch angle does not adequately correct this distortion. This distorted distribution results from the relative camera posture, as shown in Figure 5. Figure 5 illustrates how different camera pitch angles affect the shape of the PCD distribution. As the pitch angle deviates from 0°, the PCD distribution becomes distorted, leading to inaccuracies in calculating joint angles from this distorted PCD distribution. Therefore, accurate calculations of joint angles necessitate an accurate shape of the PCD distribution.

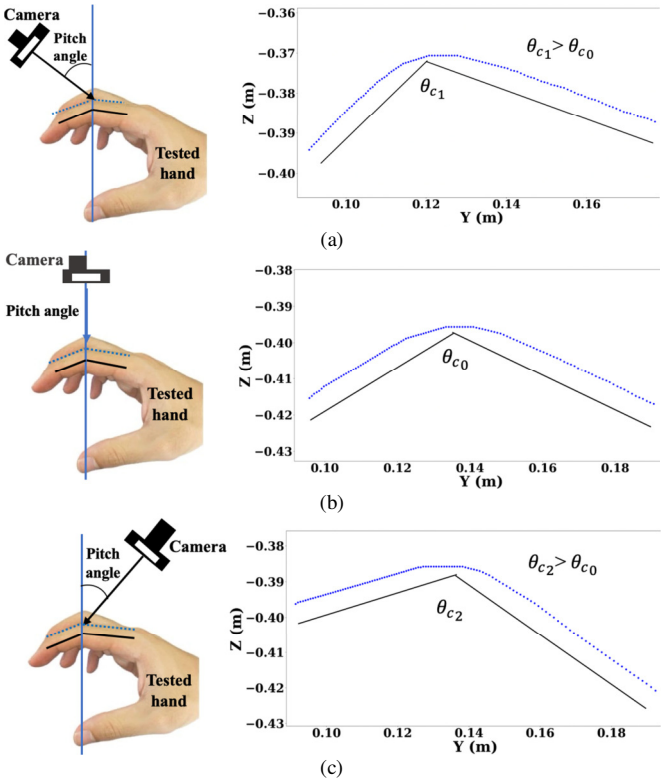

Fig. 5. Influence of the pitch angle on the 3D measurement centerline: (a) negative pitch angle, (b) zero pitch angle, and (c) positive pitch angle. (The black line represents the approximate bone axis along the longitudinal direction).

In this section, we introduce an autocorrection method designed to rectify the shape distortion caused by a camera setup with a non-zero pitch angle, with the aim of improving the shape accuracy. This approach is expected to reduce the

frequency of recaptures by therapists and decrease the measurement time. It is assumed that the therapists can adjust the roll and yaw angles to approximately 0° by monitoring the camera images. Consequently, the analysis focuses solely on the y- and z-coordinates of the 60 PCD points along the measurement centerline, denoted as $y[i]$ and $z[i]$ with $i = 1, \ldots, 60$.

The pitch angle ϕ_p is calculated using the following equation, as shown in Figure 6:

$$\phi_p[^\circ] = 180 - \arctan\left(\frac{z[60]-z[1]}{y[60]-y[1]}\right) \quad (1)$$

where $y[1]$ and $z[1]$ are the coordinates of the first point on the measurement centerline, and $y[60]$ and $z[60]$ are those of the last point.

Upon rotating the coordinates $y[i]$ and $z[i]$ by the pitch angle ϕ_p, the new y- and z-coordinates of the i-th point are expressed as $y_M[i]$ and $z_M[i]$, respectively. This rotation is outlined by (2), which demonstrates how the original blue PCD in Figure 6 is transformed into the red PCD.

$$\begin{bmatrix} y_M[i] \\ z_M[i] \end{bmatrix} = \begin{bmatrix} \cos(\phi_p) & -\sin(\phi_p) \\ \sin(\phi_p) & \cos(\phi_p) \end{bmatrix} \begin{bmatrix} y[i] \\ z[i] \end{bmatrix}, i = 1, \ldots, 60 \quad (2)$$

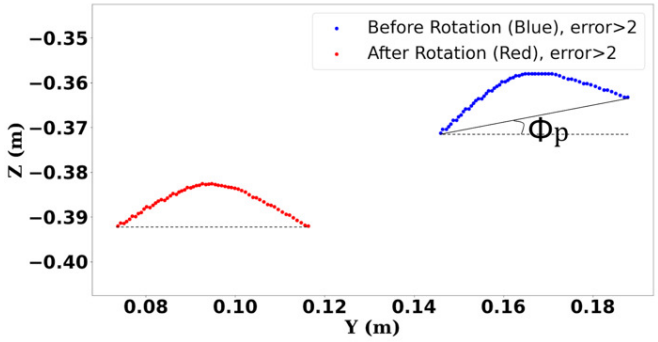

Fig. 6. Rotation method of ϕ_p to correct PCD distortion and obtain an accurate shape distribution.

Both the PCD along the measurement centerline and the PCD rotated around the x-axis exhibit distortions. To address this, we explored a correction method for the rotated PCD. Authors in [20] demonstrate adjustments made to the x- and y-coordinates to correct distortions. These distortions are associated with changes in image magnification that vary with the distance from the optical axis. Specifically, the y-coordinate of point M in the 3D PCD is adjusted based on its distance $z[i]$ from the camera. Following these insights, a coordinate transformation strategy was developed to correct the distortion. This involves a stretching transformation applied to the y-coordinates of the PCD, which is determined by the z-coordinate distance from the camera after applying the rotation matrix.

$$y_{M'}[i] = h\, y_M[i]\, z_M[i], \quad i = 1, \ldots, 60 \quad (3)$$

where $y_{M'}[i]$ and $z_{M'}[i]$ are the y- and z-coordinates of the i-th point after undergoing a stretching transformation to achieve an accurate distribution shape, with h serving as the correction parameter.

To calculate the joint angles, we employed our previously established method, utilizing the data after the stretching transformation as the measurement centerline data. The formula for calculating the candidate joint angle θ_c is:

$$\theta_c = \arccos\left(\frac{\vec{a}.\vec{b}}{|\vec{a}|.|\vec{b}|}\right), \quad (\vec{a} \neq \vec{0}, \vec{b} \neq \vec{0}) \quad (4)$$

where $\vec{a}$ is the vector of m-th to n-th points, $\vec{a} = (y_{M'}[m] - y_{M'}[n], z_{M'}[m] - z_{M'}[n])$, and $\vec{b}$ is the vector of p-th to q-th points, $\vec{b} = (y_{M'}[p] - y_{M'}[q], z_{M'}[p] - z_{M'}[q])$. We denote $m, n, p, q = 1, \ldots, 15$, so that $m > n, p > q$ to ensure that there are no overlapping vectors.

The joint angle is then calculated from all combinations of points in the PCD and a histogram is created in 1° increments. The joint angle is determined by taking the weighted average of the candidate angles with high frequencies in the distribution.

D. Design of Correction Parameter

The correction method proposed in Section II.C and denoted by (3) includes the correction parameter h, which is difficult to determine theoretically; therefore, it is derived from experimental data. In this study, the absolute error was assessed by comparing the joint angles measured by the therapist using a goniometer with the true values. Given the target accuracy for the A-ROM is within 2°, the tolerance for the measured joint angle is also set within this range. The relationship between the absolute error of the uncorrected measured joint angle, the true value, and the pitch angle is illustrated in Figure 7. When the pitch angle is within −2° to 2°, the absolute error remains within 2°. As the pitch angle deviates further from 0°, the absolute error increases. Consequently, no correction is necessary when the pitch angle lies between −2° and 2°, but corrections are required when the pitch angle exceeds these bounds. The correction parameter h is thus optimized based on these observations, with case 1 incorporating pitch angles from −30° to −2° and case 2 from 2° to 30°.

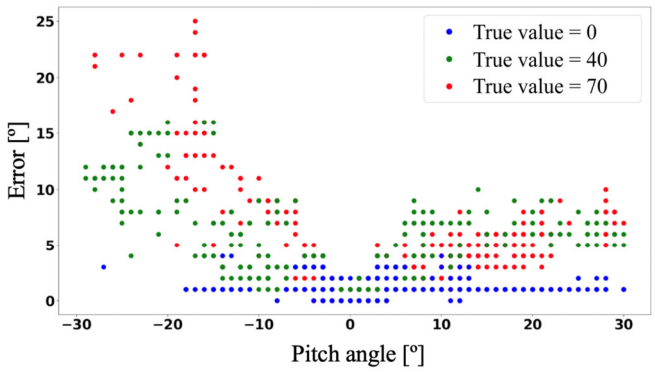

Fig. 7. Relationship between pitch angle and A-ROM calculation error for participant P1 at the PIP joint of the index finger.

For cases 1 and 2, we generated PCD from 1500 scans, adjusting 299 correction parameters (h) while analyzing the relationship between the absolute errors in joint angles and

pitch angles. From this dataset, we selected PCDs where the absolute error in joint angle was 2° or less, and plotted these data with the pitch angle on the horizontal axis and the correction parameter h on the vertical axis, as illustrated in Figure 8.

Here, 80% of the PCDs comprised the training set, with the remaining 20% serving as the test set to assess model fit. The linear regression lines are shown as red lines in Figure 8(a) and 8(b), with the regression equations for cases 1 and 2 being $h = 0.045\phi_p - 1.5$ and $h = 0.04\phi_p + 1.$, respectively. Using the 20% test set, we computed R^2 values, which yielded results of 0.93 and 0.9 for cases 1 and 2, respectively, indicating a high goodness of fit and thus validating the linear regression models.

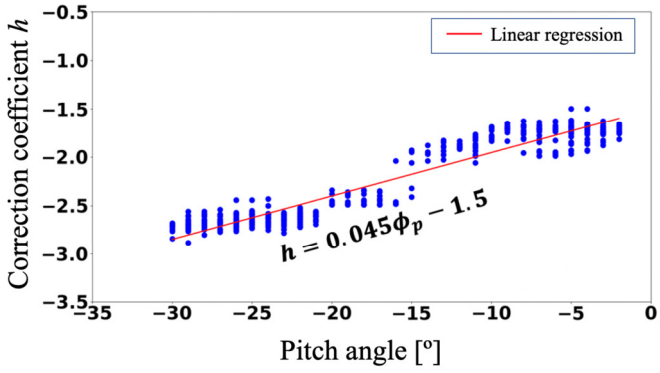

(a)

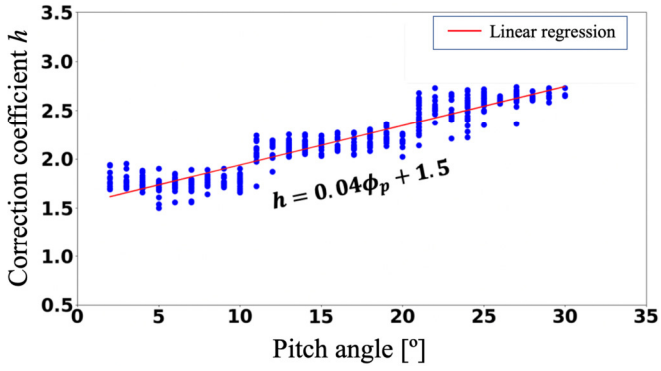

(b)

Fig. 8. Relationship between the pitch angle ϕ_p and the correction parameter h, where the absolute error in joint angle remains within 2°, along with the corresponding linear regression equation: (a) case 1 (-30°≤ϕ_p≤-2°), and (b) case 2 (2°≤ϕ_p≤30°).

III. MEASUREMENT ACCURACY VERIFICATION EXPERIMENT

A. Experimental Method

The proposed method was compared with our previous method in [15] in terms of A-ROM accuracy and measurement time. The aim of this study was to develop an alternative to the conventional goniometer, which, although widely used, requires direct contact with the patient. For evaluation purposes, the joint angles measured with a conventional goniometer were considered the true values for calculating A-ROM accuracy. Three different tests, referred to as tests A, B, and C, were conducted to represent various joint angles. These measurements captured joint angles at three points—near the minimum, middle, and maximum of the training range—using a triangular jig to maintain consistency in joint positioning during each test, as depicted in Figure 9.

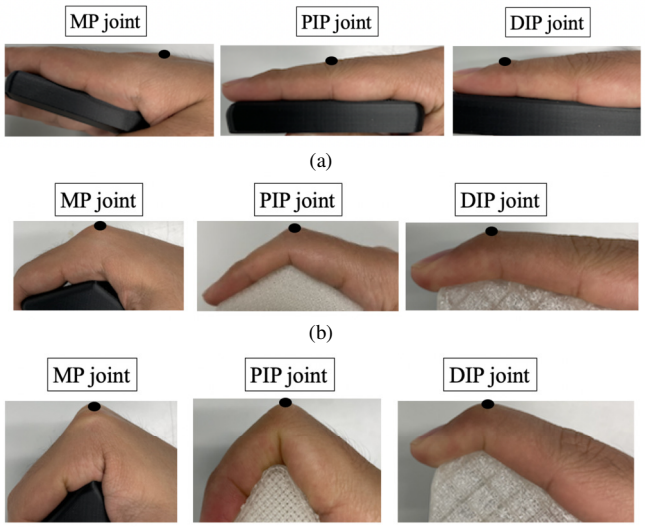

(a)

(b)

(c)

Fig. 9. Experimental validation with DIP (0°, 20°, 40°), PIP (0°, 40°, 70°), and MP (0°, 40°, 70°) joint angles: (a) test A, (b) test B, and (c) test C.

Each joint was measured independently and sequentially using both the proposed device and the conventional goniometer. Measurement time was documented as the time required for the therapist to complete the entire A-ROM measurement process, from initiating, to adjusting the camera posture relative to the target joint, culminating in the computation of the A-ROM. In addition, our previous study [15] involved only a single subject for validation. This study introduces a new method for calculating the A-ROM that takes into account individual differences in gender and hand size. As shown in Table I, five healthy subjects aged 20–30 years participated in this experiment.

TABLE I. PARTICIPANT INFORMATION

Attributes	P1	P2	P3	P4	P5
Age	30	26	24	23	22
Gender	Male	Male	Female	Female	Male

B. Experimental Results

Figure 10 illustrates the absolute error in the A-ROM for each test and participant using the proposed method. The mean error was 1.3° with a standard deviation of 1.0°. Table II presents the mean and standard deviation of the measurement times for a finger joint as recorded by both the previous [15] and the proposed methods, which were 4.9 s and 1.3 s, respectively. Consequently, the measurement time was reduced by 73.5% using the proposed device.

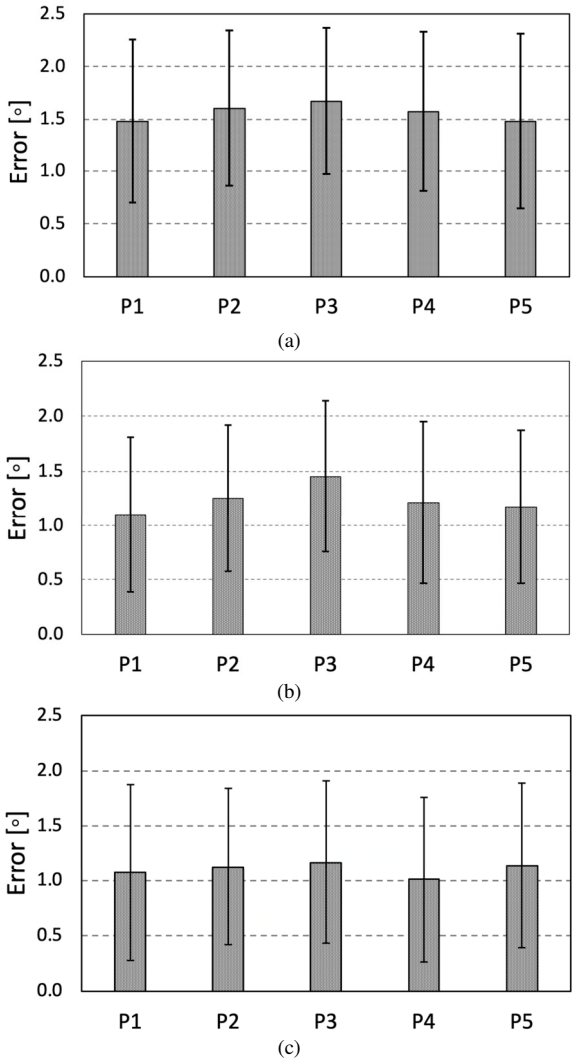

Fig. 10. Comparison of A-ROM measurement errors using the proposed method versus a conventional goniometer for five participants: (a) test A, (b) test B, and (c) test C.

IV. DISCUSSION

In this study, A-ROMs were measured for 12 finger joints. In rehabilitation, the general tolerance for measurement accuracy is within 5°, but specifically for finger joint angles, it is within 2°. The experimental results indicate that the measurement error with the proposed method is lower than that achieved with the previous method [15]. Additionally, the average A-ROM error was less than 2° for all five participants, confirming the method's ability to accommodate individual variances. Furthermore, the time required for measurement was reduced, thereby reducing the burden on both therapists and patients. Active measurement of A-ROM requires patients to extend or flex the joint with maximum effort. According to Table II, the measurement times for 12 joints in the previous study were approximately 60 s, but were reduced to approximately 15 s with the proposed method. Previously, if the pitch angle of the camera's relative posture during capture was not close to 0°, it was necessary to restart the measurement process from the beginning, as indicated by the outer loop in Figure 2. The elimination of this loop contributed significantly to the reduction in measurement times.

TABLE II. MEAN AND STANDARD DEVIATION OF MEASUREMENT TIME FOR A FINGER JOINT

Method	Mean and standard deviation of measurement time for a finger joint
Previous method [15]	4.9 ± 0.8 s
Proposed method	1.3 ± 0.4 s

Table III presents a comparison of the accuracy of this study's method with that of previous studies. The enhancements in the proposed device are considered crucial for hand therapy, particularly in evaluating the effectiveness of therapeutic interventions. This device is automated and contactless, and is designed to replace manual measurements. It reduces measurement time and alleviates the burden on both patients and therapists during the measurement process.

TABLE III. COMPARISON OF RESEARCH RESULTS

Reference	Main device	Features	Mean absolute error
[10]	Fiber Bragg grating strain sensor	Uses only sensors without cameras	1.63°
[11]	Soft strain sensors	Uses only sensors without cameras	3.5°
[13]	RGB camera	Uses a single image captured by an RGB camera without predetermined hand information. The hand image must have a resolution of at least 512 × 512 pixels. In addition, the method includes background subtraction from the hand image	4.757°
Proposed method	RGBD camera	Improves the accuracy of the A-ROM measurement for finger joint angles using an image processing and automatic computation approach	1.3°

V. CONCLUSION

This study improved the accuracy of finger joint Active Range of Motion (A-ROM) measurements based on the principle of measuring with a conventional goniometer to minimize errors caused by improper posture and camera posture, as well as distortion in the Point Cloud Data (PCD). In our previous research, the proper posture was detected using the Hand Keypoint (HKP) and Single Shot MultiBox Detector (SSD) algorithms, which required large training data. In this study, a novel Image Processing Algorithm (IPA) was introduced that not only helps to determine the proper posture and camera posture, but also detects the center points and individual differences in gender and hand size. Moreover, even when the proper posture is determined by ensuring that the roll and yaw angles are close to 0°, the pitch angle of the camera setup can still cause a large inaccuracy, which requires the therapist to restart the A-ROM measurement procedure from the first image capture step; eventually, a longer total

measurement time is traded off for accuracy. Therefore, this study ensured both the quality of the accuracy and the reduction of the device time by first introducing an auto-correction algorithm that takes into account the shape of the PCD distribution caused by the non-zero pitch angle.

The evaluation of accuracy and measurement time was also more comprehensive than our previous research by providing experiments on five different participants to account for individual variance, which was the limitation of the SSD algorithm when relying on training data. Accuracy was maintained at 1.3°, but measurement time was significantly reduced from 4.9 s to 1.3 s, representing a 73.5% reduction in time. The novelty of this research not only helps therapists to accurately and quickly measure the A-ROM of patients' finger joints, but also opens pathways for A-ROM measurement of other joints due to the universal approach of image processing and auto-correction algorithm. This method is also economical in practice by reducing the reliance on therapist expertise and large training data.

The methodology of this study outperforms comparable investigations, with a mean absolute error of 1.3° for the proposed device. Authors in [10] used a fiber Bragg grating strain sensor with an average error of 1.63°, whereas authors in [11] used soft strain sensors with an average error of 3.5°. Authors in [13] used an RGB camera with a single image requiring a minimum resolution of 512 × 512 pixels and achieved an average error of 4.757°. Thus, our approach improved accuracy using advanced technology that integrates image processing and automated computation. In future studies, a key challenge will be to improve the usability of the device and to validate its performance in clinical settings.

REFERENCES

[1] E. Lewis, L. Fors, and W. J. Tharion, "Interrater and Intrarater Reliability of Finger Goniometric Measurements," *The American Journal of Occupational Therapy*, vol. 64, no. 4, pp. 555–561, Jul. 2010, https://doi.org/10.5014/ajot.2010.09028.

[2] R. Richard, I. S. Parry, A. Santos, and W. S. Dewey, "Burn Hand or Finger Goniometric Measurements: Sum of the Isolated Parts and the Composite Whole," *Journal of Burn Care & Research*, vol. 38, no. 6, pp. e960–e965, Nov. 2017, https://doi.org/10.1097/BCR.0000000000000529.

[3] G. Legnani, B. Zappa, F. Casolo, R. Adamini, and P. L. Magnani, "A model of an electro-goniometer and its calibration for biomechanical applications," *Medical Engineering & Physics*, vol. 22, no. 10, pp. 711–722, Dec. 2000, https://doi.org/10.1016/S1350-4533(01)00009-1.

[4] Y. Ohtaki, N. Mamizuka, M. Fard, Y. Harada, Y. Minakuchi, and N. Ochiai, "Identification of Patellar Tendon Reflex Based on Simple Kinematic Measurement," *Journal of Biomechanical Science and Engineering*, vol. 4, no. 2, pp. 265–273, 2009, https://doi.org/10.1299/jbse.4.265.

[5] K. Yamada, K. Oda, and N. Tomita, "Measurement of Probe Angle for Ultrasound Evaluation of Articular Cartilage Using 'Rise-to-Peak Time,'" *Journal of Biomechanical Science and Engineering*, vol. 5, no. 5, pp. 615–624, 2010, https://doi.org/10.1299/jbse.5.615.

[6] J. R. Cook, N. A. Baker, R. Cham, E. Hale, and M. S. Redfern, "Measurements of Wrist and Finger Postures: A Comparison of Goniometric and Motion Capture Techniques," *Journal of Applied Biomechanics*, vol. 23, no. 1, pp. 70–78, Feb. 2007, https://doi.org/10.1123/jab.23.1.70.

[7] L. Reissner, G. Fischer, R. List, W. R. Taylor, P. Giovanoli, and M. Calcagni, "Minimal detectable difference of the finger and wrist range of motion: comparison of goniometry and 3D motion analysis," *Journal of Orthopaedic Surgery and Research*, vol. 14, no. 1, Jun. 2019, Art. no. 173, https://doi.org/10.1186/s13018-019-1177-y.

[8] G. M. Lim, P. Jatesiktat, C. W. Keong Kuah, and W. Tech Ang, "Camera-based Hand Tracking using a Mirror-based Multi-view Setup," in *2020 42nd Annual International Conference of the IEEE Engineering in Medicine & Biology Society*, Montreal, Canada, 2020, pp. 5789–5793, https://doi.org/10.1109/EMBC44109.2020.9176728.

[9] C. D. Metcalf *et al.*, "Markerless Motion Capture and Measurement of Hand Kinematics: Validation and Application to Home-Based Upper Limb Rehabilitation," *IEEE Transactions on Biomedical Engineering*, vol. 60, no. 8, pp. 2184–2192, Aug. 2013, https://doi.org/10.1109/TBME.2013.2250286.

[10] J. S. Kim *et al.*, "Wearable Hand Module and Real-Time Tracking Algorithms for Measuring Finger Joint Angles of Different Hand Sizes with High Accuracy Using FBG Strain Sensor," *Sensors*, vol. 20, no. 7, Apr. 2020, Art. no. 1921, https://doi.org/10.3390/s20071921.

[11] S. Lu, D. Chen, C. Liu, Y. Jiang, and M. Wang, "A 3-D finger motion measurement system via soft strain sensors for hand rehabilitation," *Sensors and Actuators A: Physical*, vol. 285, pp. 700–711, Jan. 2019, https://doi.org/10.1016/j.sna.2018.12.004.

[12] S. Mayer, M. Mayer, and N. Henze, "Feasibility analysis of detecting the finger orientation with depth cameras," in *Proceedings of the 19th International Conference on Human-Computer Interaction with Mobile Devices and Services*, Vienna, Austria, 2017, pp. 1–8, https://doi.org/10.1145/3098279.3122125.

[13] D. Viatkin, B. Garcia-Zapirain, and A. Méndez Zorrilla, "Deep Learning Techniques Applied to Predict and Measure Finger Movement in Patients with Multiple Sclerosis," *Applied Sciences*, vol. 11, no. 7, Apr. 2021, Art. no. 3137, https://doi.org/10.3390/app11073137.

[14] D. P. Tran, D. Morita, N. Sato, Y. Morita, and M. Takekawa, "Improvement of non-invasive semi-automatic test device for measurement of finger joints range of motion: Reduction in burden on therapist," in *2016 16th International Conference on Control, Automation and Systems (ICCAS)*, Gyeongju, South Korea, 2016, pp. 423–427, https://doi.org/10.1109/ICCAS.2016.7832355.

[15] H.-H. Quang, Y. Morita, N. Sato, and M. Takekawa, "Digital testing device to measure the active range of motion of finger joints using an RGB-D camera," *Journal of Biomechanical Science and Engineering*, vol. 17, no. 4, pp. 21–00337, 2022, https://doi.org/10.1299/jbse.21-00337.

[16] L. Keselman, J. I. Woodfill, A. Grunnet-Jepsen, and A. Bhowmik, "Intel RealSense Stereoscopic Depth Cameras." arXiv, Oct. 29, 2017, https://doi.org/10.48550/arXiv.1705.05548.

[17] D. Herrera C., J. Kannala, and J. Heikkilä, "Joint Depth and Color Camera Calibration with Distortion Correction," *IEEE Transactions on Pattern Analysis and Machine Intelligence*, vol. 34, no. 10, pp. 2058–2064, Oct. 2012, https://doi.org/10.1109/TPAMI.2012.125.

[18] R. Chakib, N. Mérillou, P.-J. Vincent, and S. Mérillou, "Calibrating Low-cost Structured-light 3D Sensors," in *26. International Conference in Central Europe on Computer Graphics, Visualization and Computer Vision*, Pilsen, Czech Republic, 2018, pp. 30–38, https://doi.org/10.24132/CSRN.2018.2801.4.

[19] M. Servi *et al.*, "Metrological Characterization and Comparison of D415, D455, L515 RealSense Devices in the Close Range," *Sensors*, vol. 21, no. 22, Nov. 2021, Art. no. 7770, https://doi.org/10.3390/s21227770.

[20] H. Khrouch, A. Mahdaoui, M. Merras, A. M. Hsaini, I. Chana, and A. Bouazi, "Monocular Camera Calibration based on Genetic Simulated Annealing Algorithms," *Engineering, Technology & Applied Science Research*, vol. 14, no. 6, pp. 18348–18356, Dec. 2024, https://doi.org/10.48084/etasr.8710.